measurement is performed every 5 cm in the 3.4-m test field, *B*-scans are done 70 times.

Figure 4(a) shows the image of raw data obtained without any image processing. Strong reflections near the surface are found. First, the *A*-scan process of removing an *A*-scan reference is applied to the raw data. The result is presented in Figure 4(b). The 20-cm-diameter metal pipe is clearly seen, but the rest is not clear. Finally, the process of removing the averaged *B*-scan data is applied, and the image result is displayed in Figure 4(c). As is shown, the image of the targets is parabolic in shape and three different targets are seen clearly and separately. It should be mentioned that, in this process, the interpolation between two *A*-scan data results in smoother and clearer parabolic shapes. However, it is seen that it is the difficulty of finding the target at the boundary between the sand and the clay soil is shown, as well as the difference of the depth. Therefore, the UWB GPR system has very good spatial and depth resolution. Moreover, the system is able to detect nonmetallic objects, as well as thin metal wires such as power lines in homogeneous layers, for example, in sand.

4. CONCLUSION

A new compact UWB GPR has been introduced for the detection of underground gas pipelines. In particular, a traveling-wave monopole antenna for transmitting an impulse and receiving a reflected signal has been presented. Also, the visualization technique of underground targets has been explained. The system has very good depth and spatial resolution. The results show that this system has potential applications to nondestructive testing of underground objects. In further work, the system will be tested in different materials such as clay soil.

REFERENCES

1. D.J. Daniels, Surface penetrating radar, IEE, London, 1996.
2. J.D. Taylor (Ed.), Introduction to ultra-wideband radar systems, CRC Press, Boca Raton, FL, 1995.
3. J.D. Taylor (Ed.), Ultra-wideband radar technology, CRC Press, Boca Raton, FL, 2001.
4. A.G. Yarovoy, et al., Ground penetrating impulse radar for detection of small and shallow-buried objects, Proc IGARSS'99 5 (1999), 2468–2470.
5. Y.-J. Park, et al., Development of an ultra-wideband ground penetrating radar (UWB GPR) for nondestructive testing of underground objects, IEEE Int Symp Antennas Propagat, Monterey, CA, 2004, (accepted).

COMPARISON OF THE PEANO–GOSPER FRACTILE ARRAY AND THE REGULAR HEXAGONAL ARRAY

J. N. Bogard, D. H. Werner, and P. L. Werner
The Pennsylvania State University
Department of Electrical Engineering
211A Electrical Engineering East
University Park, PA 16802

Received 2 June 2004

ABSTRACT: *A new class of modular broadband low-sidelobe arrays, based on the theory of fractile (fractal tile) geometry, has been recently introduced. In this paper, the radiation properties of the Peano–Gosper fractile array are compared to those of the conventional square and hexagonal arrays. It is demonstrated that the Peano–Gosper array has the same desirable grating-lobe conditions as the hexagonal array, while achieving a much lower overall sidelobe level.* © 2004 Wiley Periodicals, Inc. Microwave Opt Technol Lett 43: 524–526, 2004; Published online in Wiley InterScience (www.interscience.wiley.com). DOI 10.1002/mop.20523

Key words: *fractile array; Peano–Gosper array; hexagonal array; grating lobes; broadband*

1. INTRODUCTION

Several book chapters and review articles have been published in the last few years that deal with the subject of fractal-antenna engineering [1–3]. A considerable amount of this literature is devoted to novel concepts for antenna arrays that employ fractal geometries in their design. A new family of fractal arrays, known as fractile arrays, has been recently introduced in [4, 5]. This type of fractal array differs fundamentally from other types of fractal-array configurations studied previously, such as those reported in [1–3], which have regular boundaries with elements distributed in a fractal pattern on the interior of the array. A fractile array is defined as any array which has a fractal boundary contour that tiles the plane. Fractal tiles, or fractiles, represent a unique subset of all possible tile geometries that can be used to cover the plane without gaps or overlaps. The unique geometrical properties of fractiles have been exploited in [4, 5] to develop a new design methodology for modular broadband antenna arrays. Another important property of fractile arrays is that their self-similar tile geometry can be exploited to develop a rapid iterative procedure for calculating the far-field radiation patterns corresponding to these arrays.

This paper focuses on a specific type of fractile array that is based on the Peano–Gosper family of space-filling curves. The elements of the array are uniformly distributed along a Peano–Gosper curve, which leads to a planar-array configuration with a hexagonal lattice on the interior that is bounded by an irregular closed Koch fractal curve around its perimeter. These unique properties were exploited in [4] to develop a design methodology for deterministic low-sidelobe arrays that have no grating lobes, even when the minimum spacing between elements is increased to one wavelength. Hence, these Peano–Gosper fractile arrays are relatively broadband, as compared to more conventional periodic planar arrays that have a square lattice on the interior and regular boundary contours. In this paper, the radiation characteristics of Peano–Gosper fractile array are compared with those of the conventional square and hexagonal arrays. This comparison leads to a deeper fundamental understanding of the highly desirable properties exhibited by the Peano–Gosper and related family of fractile arrays.

2. THE HEXAGONAL AND PEANO–GOSPER ARRAY GEOMETRIES

The conventional hexagonal array is composed of elements arranged in an equilateral triangular lattice, sometimes referred to as a regular hexagonal lattice. The radiation properties of hexagonal arrays have been well documented in [6, 7]. More recently, the Peano–Gosper fractile array, along with the iterative process used to generate it, were introduced in [4]. Figure 1 shows the relationship between the geometry of a 352-element hexagonal array and the stage-3 Peano–Gosper fractile array that contains a total of 344 elements. The element locations of the hexagonal array are represented by an "×" while the locations of the stage 3 Peano–Gosper fractile array elements are represented by a "+". This figure demonstrates that the interior of the Peano–Gosper fractile array consists of a hexagonal lattice of elements, while the elements

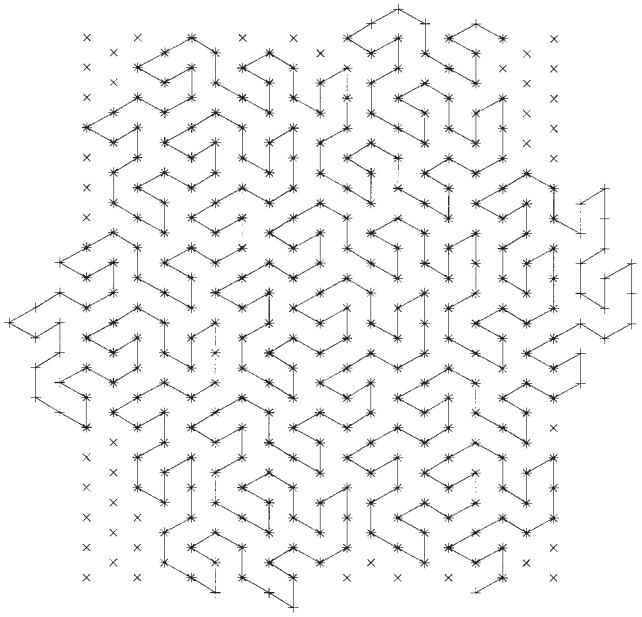

Figure 1 Element locations for a stage-3 Peano–Gosper fractile array (344 elements) and a 352-element hexagonal array

around its periphery follow an irregular Koch-fractal type of distribution.

Peano–Gosper fractile arrays may be iteratively constructed to any arbitrary stage of growth P based on a set formula for copying, scaling, rotating, and translating the generating array defined at stage 1. This fact has been used in [4] to show that the array factor for a stage P Peano–Gosper fractile array may be conveniently expressed in terms of the product of P 3×3 matrices $\boldsymbol{B}_P$, which are premultiplied by a vector $\boldsymbol{A}_P$ and post-multiplied by a vector $\boldsymbol{C}$. The general form of the resulting expression for the stage P array factor is given by

$$AF_P(\theta, \varphi) = \boldsymbol{A}_P \boldsymbol{B}_P \boldsymbol{C}, \tag{1}$$

$$\boldsymbol{A}_P = [a_1^P \quad a_2^P \quad a_3^P], \tag{2}$$

$$\boldsymbol{C} = [1 \quad 0 \quad 0]^T, \tag{3}$$

$$\boldsymbol{B}_P = \prod_{p=1}^{P} \boldsymbol{F}_P = \boldsymbol{B}_{P-1} \boldsymbol{F}_P, \tag{4}$$

$$\boldsymbol{F}_P = [f_{ij}^p]_{(3\times 3)}. \tag{5}$$

The hexagonal array can be conveniently decomposed into two interlaced rectangular-lattice arrays. The array factor for the hexagonal array can then be readily determined by the superposition of the radiation patterns from the two interlaced rectangular arrays [6]. Moreover, the examples of Peano–Gosper, hexagonal, and square arrays considered in the following section are assumed to be uniformly excited and phased for broadside operation.

3. RESULTS

In this section, we compare the radiation characteristics of the Peano–Gosper fractile array with the conventional square-lattice and hexagonal-lattice arrays. Plots of the normalized array factor versus θ for a 19×19 square array (dotted curves), 352-element hexagonal array (solid curves), and the stage-3 Peano–Gosper fractile array with 344 elements (dashed curves) are shown in Figures 2 and 3 for $\varphi = 0°$ and $\varphi = 90°$, respectively. All three arrays are comparable in size with the spacing between elements for each case, set to one wavelength (that is, $d_{\min} = \lambda$).

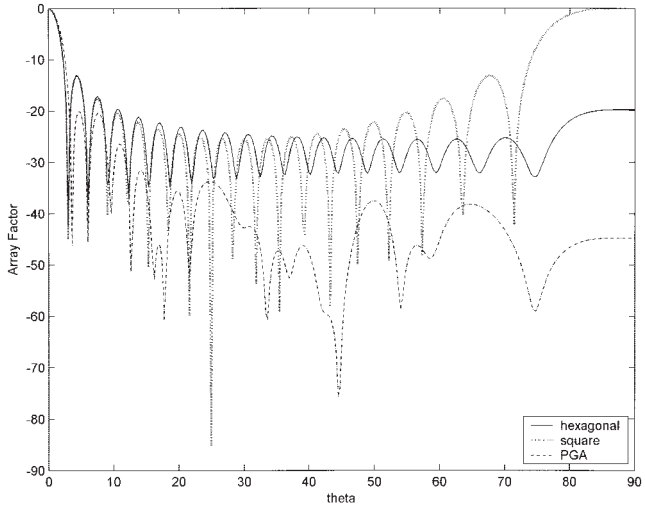

Figure 2 Plots of the normalized array factor vs. θ in degrees with $\varphi = 0°$ when the element spacing is $d_{\min} = \lambda$ for a 19×19 square array, a 352-element hexagonal array, and a 344-element stage-3 Peano–Gosper array (PGA)

The dotted curves shown in Figures 2 and 3 clearly demonstrate that grating lobes are present in the radiation pattern of the 19×19 square array. On the other hand, the corresponding radiation pattern cuts for the hexagonal and the Peano–Gosper arrays do not exhibit grating lobes in either plane. In fact, it can be shown that the desirable grating-lobe properties of the hexagonal array are shared by the Peano–Gosper fractile array. This is due to the fact that the elements on the interior of the Peano–Gosper array are arranged in a regular hexagonal lattice. However, the array factor plots shown in Figures 2 and 3 also demonstrate that the Peano–Gosper fractile array has much lower sidelobe levels than the

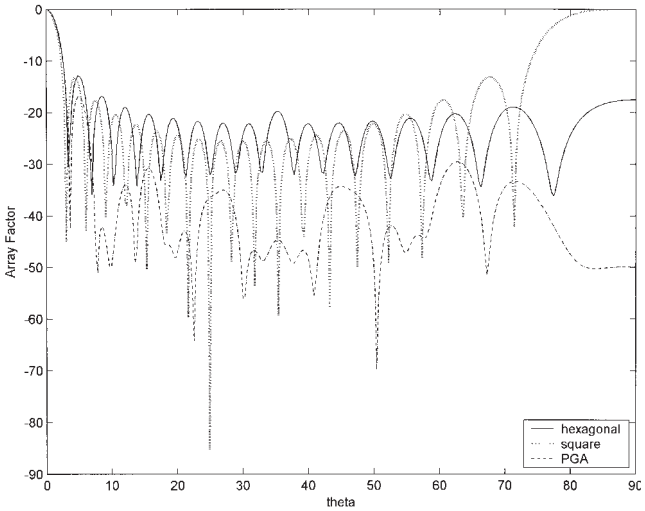

Figure 3 Plots of the normalized array factor vs. θ in degrees with $\varphi = 90°$ when the element spacing is $d_{\min} = \lambda$ for a 19×19 square array, a 352-element hexagonal array, and a 344-element stage-3 Peano–Gosper array (PGA)

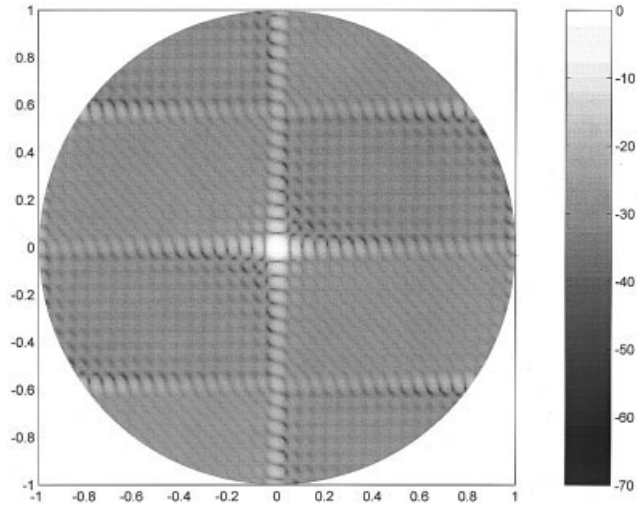

Figure 4 Contour plot of the normalized radiation pattern for a 352-element hexagonal array

hexagonal array, even though both arrays are uniformly excited. This highly desirable property of Peano–Gosper arrays is a direct consequence of the irregular Koch fractal boundaries that they possess. Contour plots of the normalized array factors for the 352-element hexagonal array and the 344-element stage-3 Peano–Gosper fractile array are shown in Figures 4 and 5, respectively, for the entire visible region. These plots further illustrate that there are no grating lobes anywhere in the visible region of either array, and that the Peano–Gosper array has a considerably lower overall sidelobe level than its hexagonal-array counterpart.

Table 1 provides a comparison between the maximum directivity of a conventional 19 × 19 square array (361 elements), a 352-element hexagonal array, and a stage-3 Peano–Gosper fractile array with 344 elements. These directivity comparisons are made for three different element spacings. In the first case, where the element spacing is $d_{\min} = \lambda/4$, the maximum directivity of the three arrays is comparable. The maximum directivity is also comparable when the element spacing is increased to $d_{\min} = \lambda/2$. However, in the third case, when the element spacing is increased to $d_{\min} = \lambda$, the maximum directivity for a stage-3 Peano–Gosper

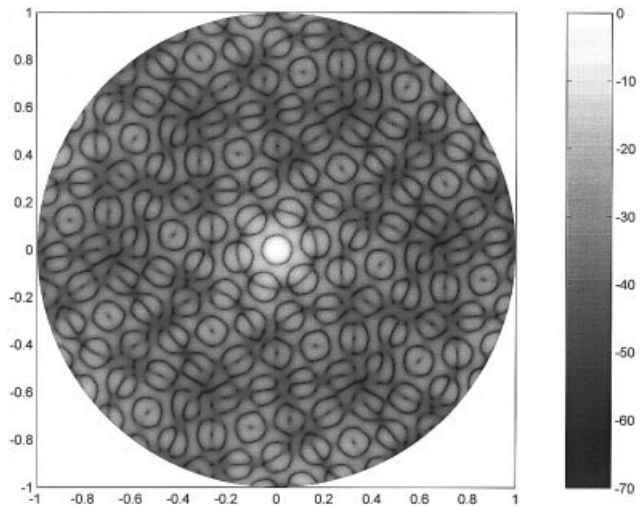

Figure 5 Contour plot of the normalized radiation pattern for a stage-3 Peano–Gosper fractile array with 344 elements

TABLE 1 Comparison of the Maximum Directivity (dBi) for a 19 × 19 Square Array, 352-Element Hexagonal Array, and a Stage-3 Peano–Gosper Fractile Array with 344 Elements

Maximum Directivity (dBi)			
Element Spacing $d_{\min}/\lambda$	19 × 19 Square Array	352-Element Hexagonal Array	Stage-3 Peano–Gosper Array
.25	21.42	20.54	20.67
.5	27.36	25.61	26.54
1	21.27	28.42	31.25

fractile array is about 10 dBi higher than the 19 × 19 square array and about 3 dBi higher then the 352-element hexagonal array. Moreover, the maximum directivity of the 19 × 19 square array drops from 27.36 to 21.27 dBi when the element spacing is changed from a half wavelength to one wavelength, while on the other hand, the maximum directivity of the 352-element hexagonal array and the stage-3 Peano–Gosper fractile array both increase. The drop in value of maximum directivity for the 19 × 19 square array may be attributed to the appearance of grating lobes in the radiation pattern.

4. CONCLUSIONS

In this paper, the radiation characteristics of a uniformly excited broadside Peano–Gosper fractile array have been compared to those of a conventional hexagonal and square array. It was shown that the Peano–Gosper array has the same desirable grating-lobe conditions as the hexagonal array, due to the fact that the elements are arranged in an equilateral triangular lattice on its interior. It was also shown, however, that the Peano–Gosper array has a considerably lower overall sidelobe level than the hexagonal array, as well as higher maximum directivity for element spacings of one wavelength. These highly desirable properties of Peano–Gosper arrays are a direct consequence of their irregular Koch fractal boundaries.

REFERENCES

1. D.H. Werner, R.L. Haupt, and P.L. Werner, Fractal antenna engineering: The theory and design of fractal antenna arrays, IEEE Antennas Propagat Mag 41 (1999), 37–59.
2. D.H. Werner and R. Mittra (Eds.), Frontiers in electromagnetics, IEEE Press, Piscataway, NJ, 2000.
3. D.H. Werner and S. Ganguly, An overview of fractal antenna engineering research, IEEE Antennas Propagat Mag 45 (2003), 38–57.
4. D.H. Werner, W. Kuhirun, and P.L. Werner, The Peano–Gosper fractal array, IEEE Trans Antennas Propagat 51 (2003), 2063–2072.
5. D.H. Werner, W. Kuhirun, and P.L. Werner, Fractile arrays: A new class of tiled arrays with fractal boundaries, IEEE Trans Antennas Propagat (accepted).
6. A.W. Rudge, K. Milne, A.D. Olver, and P. Knight (Eds.), The handbook of antenna design, Peter Peregrinus Ltd., London, 1986.
7. Y.T. Lo and S.W. Lee (Eds.), Antenna handbook: Theory, applications, and design, Van Nostrand Reinhold Company, New York, 1988.